

Precession phasing offset between Indian summer monsoon and Arabian Sea productivity linked to changes in Atlantic overturning circulation

Martin Ziegler,^{1,2} Lucas J. Lourens,¹ Erik Tuenter,³ Frits Hilgen,¹ Gert-Jan Reichart,¹ and Nanne Weber⁴

Received 5 November 2009; revised 9 April 2010; accepted 21 April 2010; published 9 September 2010.

[1] Results from transient climate modeling experiments indicate an in-phase relationship between insolation forcing and Indian summer monsoonal precipitation. This is in contrast to high-resolution radioisotopically dated speleothem oxygen isotope ($\delta^{18}\text{O}$) records of China, which showed that East Asian Monsoon maxima lag Northern Hemisphere peak summer insolation by $\sim 2,700$ years, while an approximately 8,000-year time lag was derived from late Pleistocene records of Arabian Sea sediments. Here, we evaluate the precession phase of the Arabian Sea signal by comparing a new high-resolution productivity and oxygen minimum zone (OMZ) intensity record from the Arabian Sea over the past 450,000 years with the results of a transient climate modeling experiment that includes glacial-bound ice volume variations. The well established tuning technique between radioisotopically dated North Atlantic cold events and the occurrence of deep-dwelling planktonic foraminifera in the Arabian Sea for the last glacial cycle was used to extend the Arabian Sea chronology, independent of orbital tuning. Cross-spectral analysis over the last 224,000 years reveals that Arabian Sea productivity maxima lag precession minima by $\sim 6,900 \pm 200$ years, i.e., in close agreement with previous reconstructions. Also our climate modeling simulations are in accord with previous studies indicating an in-phase relationship between precession minima and maximum summer monsoon intensity. We argue that the summer monsoon is most likely not the main driver of changes in Arabian Sea biological productivity and OMZ intensity at the precession frequency band, but that changes in the intensity of the Atlantic meridional overturning circulation (AMOC) have played the prominent role in controlling the nutrient delivery into the euphotic layer of the northern Indian Ocean, and hence the amount of primary productivity and intensity of the oxygen minimum zone in the Arabian Sea. Such a mechanism explains the large precession-related time lag between minimum precession and maximum productivity and OMZ conditions in the Arabian Sea, since intensified AMOC occurred during precession maxima.

Citation: Ziegler, M., L. J. Lourens, E. Tuenter, F. Hilgen, G.-J. Reichart, and N. Weber (2010), Precession phasing offset between Indian summer monsoon and Arabian Sea productivity linked to changes in Atlantic overturning circulation, *Paleoceanography*, 25, PA3213, doi:10.1029/2009PA001884.

1. Introduction

[2] Paleostudies from the Arabian Sea have indicated an exceptionally long precession-related time lag between northern hemisphere peak summer insolation and maximum productivity and oxygen-minimum-zone (OMZ) intensity of approximately 8,000 years [Clemens *et al.*, 1996; Clemens and Prell, 2003; Reichart *et al.*, 1998; P. Wang *et al.*, 2005]. Because upwelling-driven productivity is com-

monly linked to the Indian summer monsoon intensity, it has been proposed that this large time lag resulted from the maximum latent heat transport of the Southern Ocean toward the Asian continent [Clemens *et al.*, 1996; Clemens and Prell, 2003]. As alternative it has been suggested that productivity exhibits a long lag due to a response to late summer insolation, building on the observation that modern seasonal productivity peaks are bound to the late summer [Reichart *et al.*, 1998]. Such a scenario was doubted by others, because seasonal signals cannot simply be extrapolated to orbital timescales as they are related to inertia in the system that produces lags of a few weeks and thus do not have to occur synchronously with the real forcing [Clemens *et al.*, 1996; Clemens and Prell, 2003]. A third explanation emphasizes that Arabian Sea summer monsoon proxies are not tightly coupled to the monsoon intensity but instead are influenced by other processes [Ruddiman, 2006].

[3] The general agreement between the different reconstructions of the monsoon phase lag from the marine realm stands

¹Faculty of Geosciences, Utrecht University, Utrecht, Netherlands.

²Now at Lamont-Doherty Earth Observatory, Columbia University, Palisades, New York, USA.

³Institute for Marine and Atmospheric Research Utrecht, Utrecht University, Utrecht, Netherlands.

⁴Chemistry and Climate Division, Royal Netherlands Meteorological Institute, De Bilt, Netherlands.

in sharp contrast with the outcome of climate modeling sensitivity experiments. These simulations indicate that maximum precipitation conditions over the southeast Asian continent during June–July–August (JJA) are highly coherent and in-phase with June insolation maxima (i.e., precession minima) [Kutzbach et al., 2008; Tuenter et al., 2005]. A recently achieved high-resolution, radioisotopically dated oxygen isotope ($\delta^{18}\text{O}$) record from the Sanbao and Hulu caves in China exhibits a relatively short lag behind precession minima of approximately 2,700 years [Wang et al., 2008]. Therefore, it was suggested [Wang et al., 2008] that the long time lag derived from the Arabian Sea sedimentary records could be intrinsic to their underlying SPECMAP oxygen isotope chronology [Imbrie et al., 1984, 1992, 1993]. In fact, high-precision radioisotopic studies pointed out that the SPECMAP based phase lags are probably overestimated and thus that orbitally tuned late Pleistocene benthic $\delta^{18}\text{O}$ chronologies generate ages which are probably several thousand years too young [Gallup et al., 2002; Henderson and Slowey, 2000; Winograd et al., 1992], although, another study supported the SPECMAP chronology [Thompson and Goldstein, 2006].

[4] Our paper has three main objectives: First we will evaluate whether the chronology could indeed be responsible for the exceptional long phase lag in the Arabian Sea records. Second, we will test in a climate modeling study if the incorporation of glacial-interglacial ice-volume variations can influence the precession phase of the Indian summer monsoon intensity. And third, we will discuss the importance of monsoon-independent, oceanic circulation related processes influencing the orbital signatures in the Arabian Sea productivity and OMZ records.

[5] We have measured at high-resolution changes in marine organic carbon using XRF-scanning Bromine counts [Ziegler et al., 2008] on a spliced sedimentary record of the Murray Ridge at a water depth of ~ 920 m for the last 450,000 years. Variations in organic carbon content at these shallow to intermediate water depths in the northern Arabian Sea appeared to be very sensitive to millennial-scale changes in sea surface productivity and OMZ intensity [Reichart et al., 1998; Schulz et al., 1998]. For our time scale, we correlated the occurrence of deep-dwelling planktonic foraminifera in the Arabian Sea to cold events in the North Atlantic [Reichart et al., 1998], using up-to-date radioisotopic constraints on the timing of the North Atlantic cold events. This chronology has subsequently been used to establish the precession phase of upwelling driven productivity and OMZ variability in the Arabian Sea over the past 450,000 years. In addition, we compare our results with a transient climate modeling experiment (S. L. Weber and E. Tuenter, The impact of varying ice sheets and greenhouse gases on the intensity and timing of boreal summer monsoons, submitted to *Quaternary Science Reviews*, 2010) for the whole studied interval, which unlike previous studies [Tuenter et al., 2005; Kutzbach et al., 2008] takes into account a possible influence of glacial-interglacial ice sheet fluctuations on the strength of the Indian monsoon.

2. Climatic and Oceanographic Setting

[6] Today's Arabian Sea hydrography and biogenic particle fluxes experience large seasonal variations due to strong monsoonal winds. The monsoon circulation causes cool, dry winters and warm, wet summers over the Indian subcontinent. The Indian summer monsoon is driven by differential heating of the Eurasian continent and the Southern Indian Ocean [Webster et al., 1998]. This results in a strong pressure gradient between a low-pressure cell over the Tibetan Plateau and a high-pressure cell over the Indian Ocean that generates the low-level monsoonal wind from June to September. In particular the intense Findlater Jet transports large quantities of moisture, which results in heavy rainfall over India. The release of latent heat additionally acts as a positive feedback mechanism and strengthens the surface low pressure over the Asian land-mass [Webster et al., 1998]. From January until March a reversed pressure gradient generates the dry and cold northeast winter monsoon.

[7] The seasonal changes in atmospheric circulation and precipitation also affect the Indian Ocean, leading to strong seasonality in current strength and direction, sea-surface temperature and salinity patterns. During the summer months the upper ocean currents are driven northward by the summer monsoon winds. The reversed wind direction in winter is accompanied by a reversal of the surface currents and suppressed upwelling. Upwelling of nutrient-rich intermediate waters along the coasts of Somalia and Oman make the Arabian Sea one of the most productive areas worldwide with up to $250 \text{ gC/m}^2/\text{yr}$ [Antoine et al., 1996]. Modern intermediate water masses are influenced by the contribution of highly saline Red Sea Outflow Water (RSOW) and Persian Gulf Outflow Water (PGOW) that are centered around 800 m water depth. Below that North Indian Deep Water (NIDW) extends between approximately 1200 and 3800 m water depth. NIDW originates from aged North Atlantic Deep Water (NADW) and Circumpolar Deep Water (CDW) [van Aken et al., 2004; You, 1998]. High surface productivity rates in combination with supply of oxygen-poor intermediate waters [You, 1998] produce an intense oxygen-minimum-zone between 200 and 1200 m water depth (Figure 1).

3. Material and Methods

3.1. Composite Record

[8] We composed a high-resolution Bromine record (~ 150 years average resolution) derived from four parallel, partly overlapping cores of the Murray Ridge (piston cores NIOP 463p1, NIOP 463p2, MD04-2878) at a water depth well within the present-day OMZ (920 mbss). Piston cores NIOP463p1 and NIOP463p2 at $22^\circ 32'.9 \text{ N}$ and $064^\circ 02'.8 \text{ E}$ have been taken by the RV Tyro during the Netherlands Indian Ocean Program (NIOP) expedition in 1992 (Figure 1). In 2004, NIOP463 was revisited during the CHAMAK expedition. Two long piston cores, MD04-2878 and MD04-2882, were retrieved by the Calypso coring system of the RV Marion Dufresne. MD04-2878 is 26 m long. The uppermost 10 m were not recovered, because of coring deficiencies. The

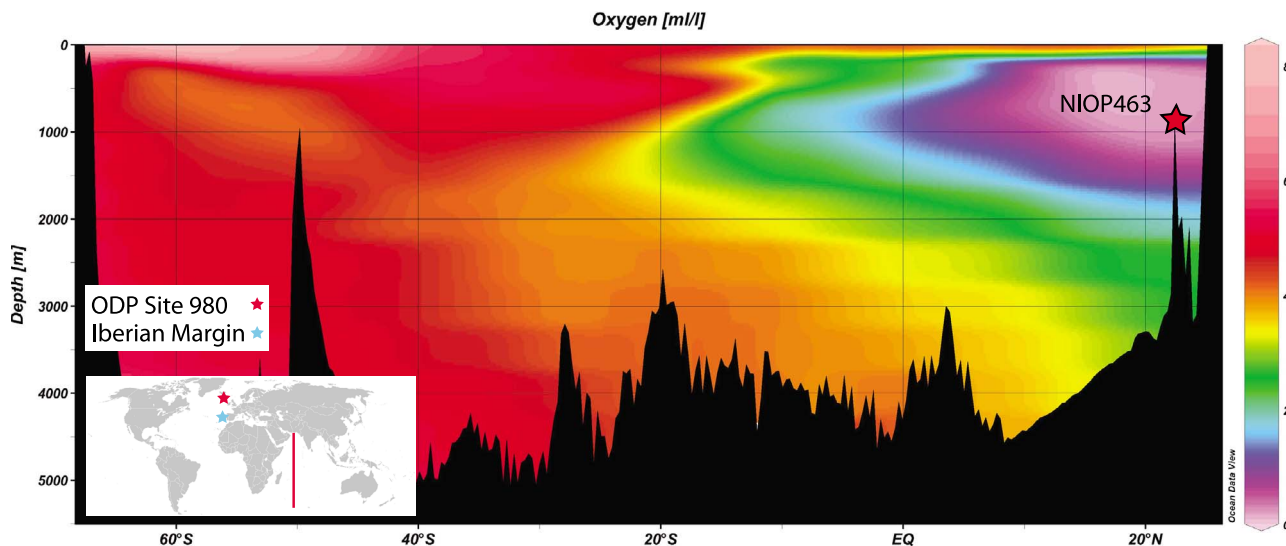


Figure 1. Location of the composite record in the Northern Arabian Sea. Oxygen profile through the Indian Ocean (World Ocean Atlas 2005 [Locarnini *et al.*, 2006] and Ocean Data View (R. Schlitzer, Ocean Data View, 2007; available at <http://odv.awi.de/>)). Star indicates position of the studied sediment cores on the Murray Ridge, northern Arabian Sea ($22^{\circ}32'.9$ N, $064^{\circ}02'.8$ E, 920 mbss) within the modern oxygen minimum zone.

lowermost 16 m stayed intact without disturbances. MD04-2882 is a 30 m long piston core, which shows some coring related disturbance structures. The Bromine XRF-scanning profile (see methods) of MD04-2882 mimics, however, the pattern observed in the other records, which sustains a complete stratigraphy. Discrete samples have been taken carefully from MD04-2882 in parts showing no or little disturbance. Comparison of the Bromine scanning data of NIOP463p1 and p2 demonstrates the high reproducibility of the Bromine XRF scans between the different cores (Figure 2). We constructed a composite record with piston cores NIOP463p1 (for the upper part) and MD04-2878 (for the lower part) as the backbone (Table 1). The data gap between the two records is filled up by the data from MD04-2882 (Figure 2). The scanning data gap in NIOP 463p1 (i.e., disturbance in the archive half of the core) has been closed using data from NIOP 463p2. Radiocarbon dates on NIOP 463 have been taken from a previous study [den Dulk *et al.*, 2000].

3.2. Analytical Methods

[9] An Avaatech XRF core scanner at the Royal Netherlands Institute of Sea Research (NIOZ, Texel, Netherlands) has been used to measure the bulk elemental composition of the sediments. The split core surface was cleaned and covered with a $4 \mu\text{m}$ thin SPEXCertiPrep Ultralene foil to avoid contamination and prevent desiccation. Each section was scanned at 0.5 milliamps (mA) and 30 kilovolts (kV). A 1 cm^2 area of the core surface was irradiated with X-rays using 30 s count time. XRF data were collected every 1 cm for all the cores except MD04-2882 which was scanned at 2 cm resolution. In order to correct for a less sensitive detector being used initially, Bromine counts of NIOP463p1 had to be multiplied with a factor of 3.75. For further

technical details on the XRF scanning technique see Richter *et al.* [2006]. We used the recently established correlation between Bromine XRF scanning counts and marine organic carbon content (MOC) to estimate the MOC variability in the sediment cores [Ziegler *et al.*, 2008].

[10] For the stable carbon and oxygen isotope ($\delta^{13}\text{C}$ and $\delta^{18}\text{O}$) analysis 20–25 specimen of the planktonic foraminiferal species *Neogloboquadrina dutertrei* were hand-picked from the $300\text{--}350 \mu\text{m}$ size fraction. The analysis was carried out at Utrecht University stable isotope facility where an ISOCARB common bath carbonate preparation device linked online to VG SIRA24 mass spectrometer is operated. Isotope values were calibrated to the Vienna Pee Dee belemnite (VPDB) scale, through analyses of National Bureau of Standards 19 reference material. Analytical precision was determined by replicate analyses and by comparison to the international (IAEA-CO1) and in-house carbonate standard (NAXOS). Replicate analyses showed standard deviations of ± 0.06 and ± 0.1 for $\delta^{13}\text{C}$ and $\delta^{18}\text{O}$, respectively.

[11] Total numbers of the deep dwelling planktonic foraminiferal species *Globorotalia truncatulinoides* and *Globorotalia crassaformis* were counted on samples from NIOP463p1, NIOP463p2, MD04-2878, and MD04-2882 on splits of the 150 to $600 \mu\text{m}$ fraction. Counts are expressed as number per gram sediment (Figure 3).

[12] Power spectra were calculated with the REDFIT software [Schulz and Mudelsee, 2002]. Spectral amplitude was estimated using the Lomb-Scargle Fourier Transform for unevenly spaced data, a Welch window and two overlapping (50%) segments; red-noise boundaries were estimated as upper 80, 90 and 95% chi-square limits of a fitted AR1-process. Phase estimates and coherences were calcu-

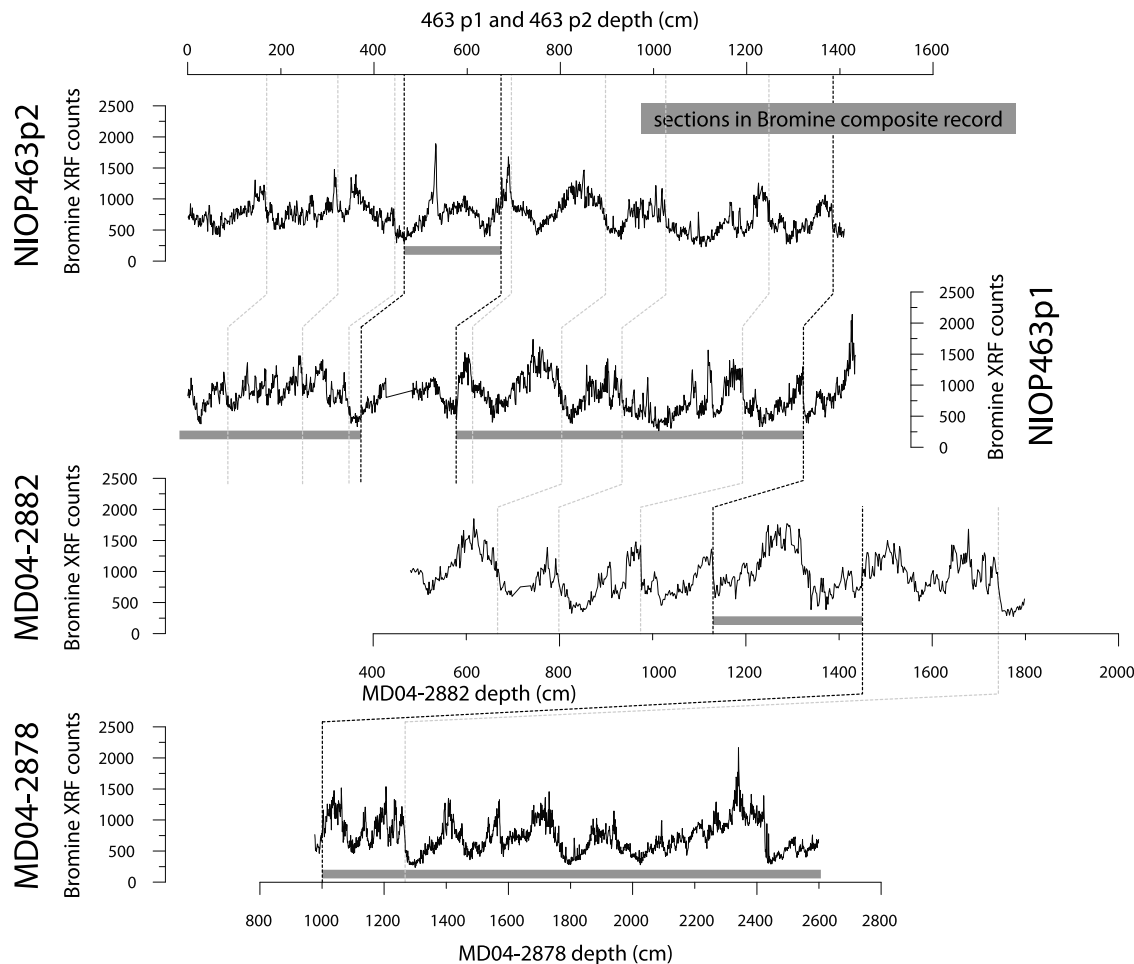


Figure 2. Down-core profiles of Bromine XRF count records of NIOP463p2, NIOP463p1, MD04-2882, and MD04-2878. Stippled lines indicate anchor horizons used to construct the composite record. Grey bars indicate sections of the individual cores, which have been used in the composite record.

lated with the Blackman-Tukey method using the *Analyseries* software [Paillard *et al.*, 1996].

4. Transient Climate Modeling Experiments

[13] To simulate changes in Indian summer monsoon precipitation we used a climate model of intermediate complexity, CLIMBER-2, version 3 [Petoukhov *et al.*, 2000], that is suitable for long transient simulations due to its fast turnaround time. The modeling experiment is discussed in detail by Tuenter *et al.* [2005] and Weber and Tuenter (submitted manuscript, 2010). The model consists

of a statistical-dynamical atmosphere, a multibasin zonally averaged ocean including sea-ice and a dynamical model of terrestrial vegetation. The atmosphere has a coarse resolution of 10° in latitude and approximately 51° in longitude. The model has been shown to capture the monsoon response to orbital forcing reasonably well, with an enhanced seasonal cycle of insolation giving rise to an intensification of NH summer monsoons [Ganopolski *et al.*, 1998b]. Results of CLIMBER-2 for the glacial climate, where continental ice sheets play an important role, also compare favorably with data as well as with results of more comprehensive models [Ganopolski *et al.*, 2001].

[14] With CLIMBER-2 we performed two transient simulations for the interval from 650 kyr BP to present (only the last 450,000 years are shown and discussed in this paper). The forcing used in the ‘orbital-only’ simulation is insolation changes induced by the $La04_{(1,1)}$ orbital parameters while ice sheets were kept fixed at present-day values. In the ‘orbital-ice’ simulation the same orbital forcing was used, but now varying ice sheets on the Northern Hemisphere were included. In contrast to Calov *et al.* [2005] we do not use an interactive ice sheet model, but we prescribed the ice

Table 1. Depth Intervals of the Composite Core

Core Name	Depth (cmbsf)		Composite Depth (cm)	
	Top	Bottom	Top	Bottom
NIOP463p1	0	396	0	396
NIOP463p2	500.5	700.5	397	597
NIOP463p1	613	1321.5	598	1306.5
MD04-2882	1054	1376	1307.5	1629.5
MD04-2878	1002	2599	1630.5	3227.5

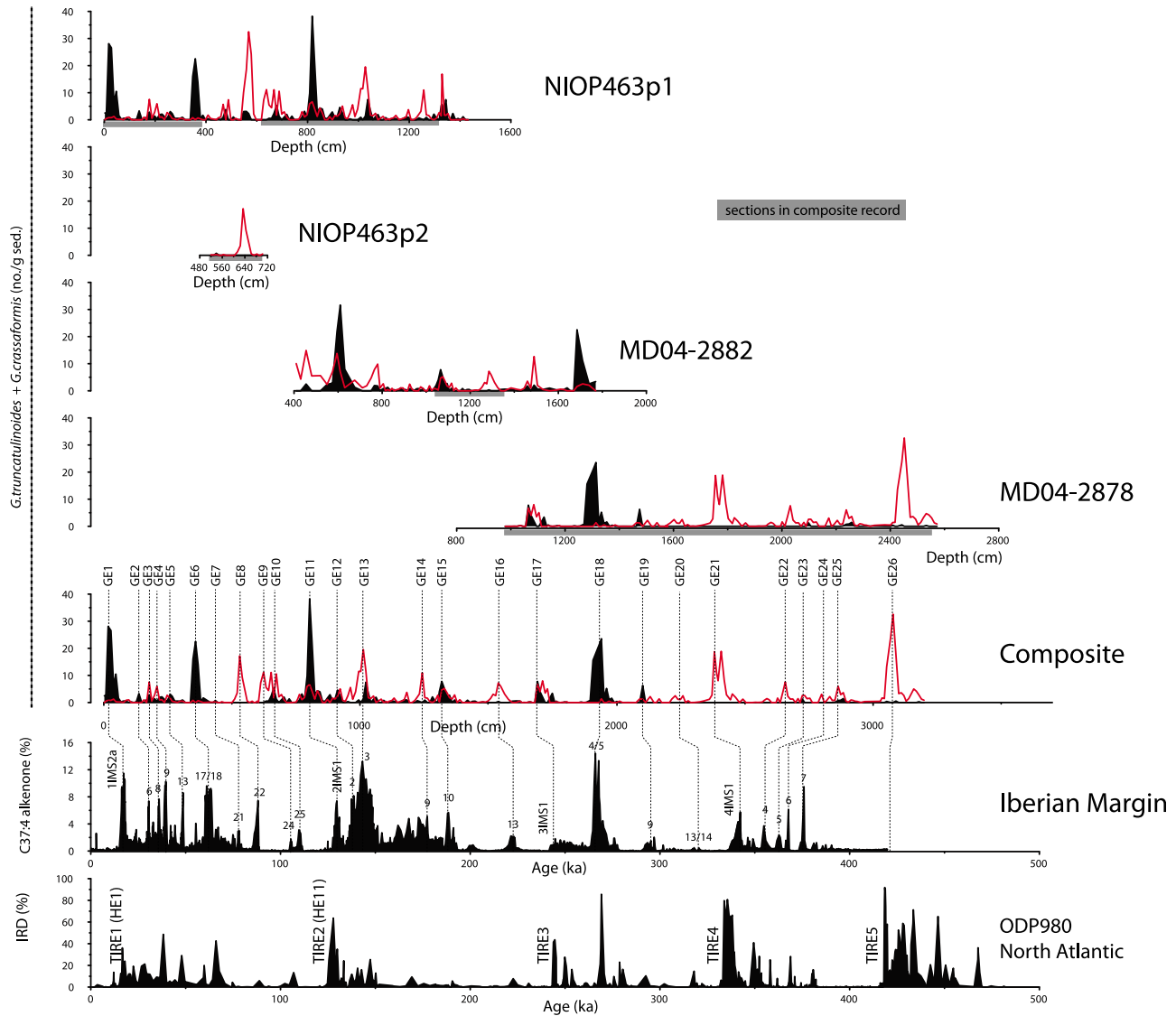


Figure 3. Down-core profiles of *G. crassaformis* (red lines) + *G. truncatulinoides* (black filled areas) (no./g sed.) of NIOP463p1, NIOP463p2, MD04-2882 and MD04-2878 and Iberian Margin alkenone (C_{37:4} (%)) record and ODP site 980 IRD (%) record. GEs are major *Globorotalia* events in the Arabian Sea. TIREs are terminal ice rafting events at glacial terminations, and IMS's are Iberian Margin stadials. HEs are Heinrich events.

fraction and height of the Eurasian and North American ice sheet. Time series of ice sheet volumes were obtained from an earlier simulation with a 3-dimensional model of the Eurasian and North American ice sheets [Bintanja et al., 2005]. Volumes were translated into ice areas and heights, needed as boundary condition for the climate model, as follows. For the ice areas the ice distribution of the Last Glacial Maximum (21 kyr BP) was used as a reference [Peltier, 2004] and translated to the resolution of CLIMBER-2 [Ganopolski et al., 1998a] (Table 2). Together with the prescribed volumes the heights H_{am} and H_{eur} of the American and the Eurasian ice sheet, respectively, can now be computed. To avoid a uniform height, we let the ice sheets at some (central) grid boxes have height H_{eur} and

H_{am} , while the ice sheets at the surrounding grid boxes have height $0.5 \cdot H_{eur}$ and $0.5 \cdot H_{am}$ (Table 2). A drawback of this method would be that only the height of the ice sheets change in time while the areas of the ice sheets are fixed at LGM values. To remedy this, we instantly lower the ice fraction of every grid box covered by ice by 0.25 when the height becomes less than 1000 m and by 0.5 when it becomes less than 500 m. So both the height of the ice sheet and the area occupied by ice (and associated albedo) vary with time. However, due to the relative coarse spatial resolution of the model and the way ice volume changes are prescribed, ice sheet height is more sensitive to smaller scale ice volume variations, whereas the aerial extent of the ice sheets changes more rapidly at the larger terminations and

Table 2. Ice Areas and Ice Heights as Prescribed in the CLIMBER-2 Modeling Experiment

Grid Box American Ice Sheet	Land Fraction	Ice Fraction	Height (in H_{am})
160W–110W; 60N–70N	1	0.5	0.5
160W–110W; 50N–60N	0.2	1	0.5
110W–60W; 70N–80N	0.7	1	0.5
110W–60W; 60N–70N	0.7	1	1
110W–60W; 50N–60N	1	1	1
110W–60W; 40N–50N	1	0.5	0.5
Grid Box Eurasian Ice Sheet	Land Fraction	Ice Fraction	Height (in H_{eur})
10W–40E; 70N–80N	0.9	1	1
10W–40E; 60N–70N	0.9	1	1
10W–40E; 50N–60N	1	0.5	0.5
40E–90E; 70N–80N	0.9	1	1
40E–90E; 60N–70N	1	0.5	1

inceptions. As a result of this, some of the precession scale variability in the ice volume is translated into ice sheet height changes rather than changes in the aerial extent of the ice sheets (see auxiliary material).¹ During the (prescribed) waxing and waning of the ice sheets there is no transport of water from the oceans to the ice sheets and vice versa.

[15] For the ‘orbital’ and the ‘orbital-ice’ simulations the height and surface area of Greenland and Antarctica as well as small glaciers were kept at present-day values. The CO_2 -concentrations were also kept fixed at a value of 280 ppmv. Both simulations have been carried out with the coupled atmosphere-ocean-vegetation system. The influence of interactive vegetation on the transient behavior of climate is described by *Tuenter et al.* [2005]. The initial states were obtained by performing a 5 kyr equilibrium run using the boundary conditions for 650 kyr BP. The results are shown as averages over 100 yrs as the periods of the orbital forcing and variations in ice sheet volume are much longer than 100 yrs.

[16] The outcomes of both runs display some differences in summer (June–July–August; JJA) precipitation over the Indian monsoon region (Figure 4a). While both runs are dominated by precession scale variability, the second run indicates some minor effect of the ~100 kyr glacial cyclicity (Figure 5a). Irrespective of ice volume variability, however, cross-spectral analysis of the JJA modeled precipitation record results in a consistent in-phase relation ($1.2^\circ \pm 0.8^\circ$) of the precession component with June 21st insolation. Even though potentially underrepresented precession variability in the aerial ice sheet extent might have influenced this result, the relatively small effect of the large 100 kyr glacial cycle on monsoon precipitation suggests that monsoon variability in general is not very sensitive to ice volume changes.

5. Arabian Sea Chronology and Phase Relations

5.1. SPECMAP Based Age Model

[17] Late Pleistocene variations in deep-sea benthic oxygen isotopes are generally attributed to global ice volume

¹Auxiliary materials are available in the HTML. doi:10.1029/2009PA001884.

changes and to a lesser extent to deep-sea temperature variability [*Lisiecki and Raymo*, 2005]. They provide therefore a solid stratigraphic system of marine isotope stages (MIS) that has an almost global coverage [*Martinson*, 1987], although diachroneity has been noted between individual benthic $\delta^{18}O$ records and MIS boundaries from different ocean basins [*Lisiecki and Raymo*, 2009; *Skinner and Shackleton*, 2005]. Previous studies directed at the orbital phasing of the Indian monsoon are commonly based on tuning to the SPECMAP oxygen isotope stack [*Imbrie et al.*, 1984, 1992, 1993] or similarly derived age models such as the LR04 [*Lisiecki and Raymo*, 2005].

[18] The reconstruction of a reliable benthic oxygen isotope chronology for the studied sites in the Arabian Sea (not shown) was complicated due to species-specific metabolic effects, susceptibility to changes in carbonate ion concentration, and supralysocline calcite dissolution [*Gupta et al.*, 2008; *Schmiedl and Mackensen*, 2006]. In addition, the relative shallow position of our composite record potentially allows considerable temperature effects on the benthic isotope record, while changes in Arabian Sea intermediate water masses between glacial and interglacial periods may potentially influence the isotopic signal [*Jung et al.*, 2001; *Zahn and Pedersen*, 1991].

[19] To build a chronology that is conformed to SPECMAP and related chronologies, we relied on the $\delta^{18}O$ record of *Neoglobobulimina dutertrei* as starting point (Figure 4e). However, we used our $\delta^{18}O$ record only for identifying the last five glacial terminations, because the surface water, planktonic isotope signal is sensitive to local (seasonal) temperature variations and freshwater fluxes. Comparison between different temperature proxies demonstrated for instance that temperature variations in the Arabian Sea are difficult to disentangle between glacial and interglacial periods [*Huguet et al.*, 2006; *Saher et al.*, 2009]; i.e., they are responding differently to changes in seasonality, upwelling and winter mixing in this complex environment.

[20] To circumvent the described problems and test the robustness of previous phase estimates, we established an alternative age model based on a quantitative record of the deep dwelling planktonic foraminifera species *Globorotalia truncatulinoides* and *Globorotalia crassaformis* (Figure 3). The same approach was followed in another study from a Murray Ridge core [*Jaeschke et al.*, 2009]. Radioisotopically dated peak occurrences of these species (*Globorotalia* events, *GEs*) correspond to major climatic cooling (i.e., Heinrich) events in the North Atlantic during the last glacial cycle and are associated with a strongly diminished or even completely absent OMZ in the Arabian Sea [*Reichart et al.*, 1998, 2004]. We correlated 26 *GE*-events to the North Atlantic ice rafted debris (IRD) record of ODP site 980, which was tuned to SPECMAP [*McManus et al.*, 1999] (Figure 3 and Table 3). We note that our age model infers that Arabian Sea *GE*-events and North Atlantic 980 IRD events are temporally correlative throughout the last 450,000 years, although this has only been proven radioisotopically for the last 60 kyrs.

[21] The *GE* time series, ranging from 12 to 444 ka, reveals highest spectral power in the 21-kyr band of precession, but in contrast to the IRD record less significant power was

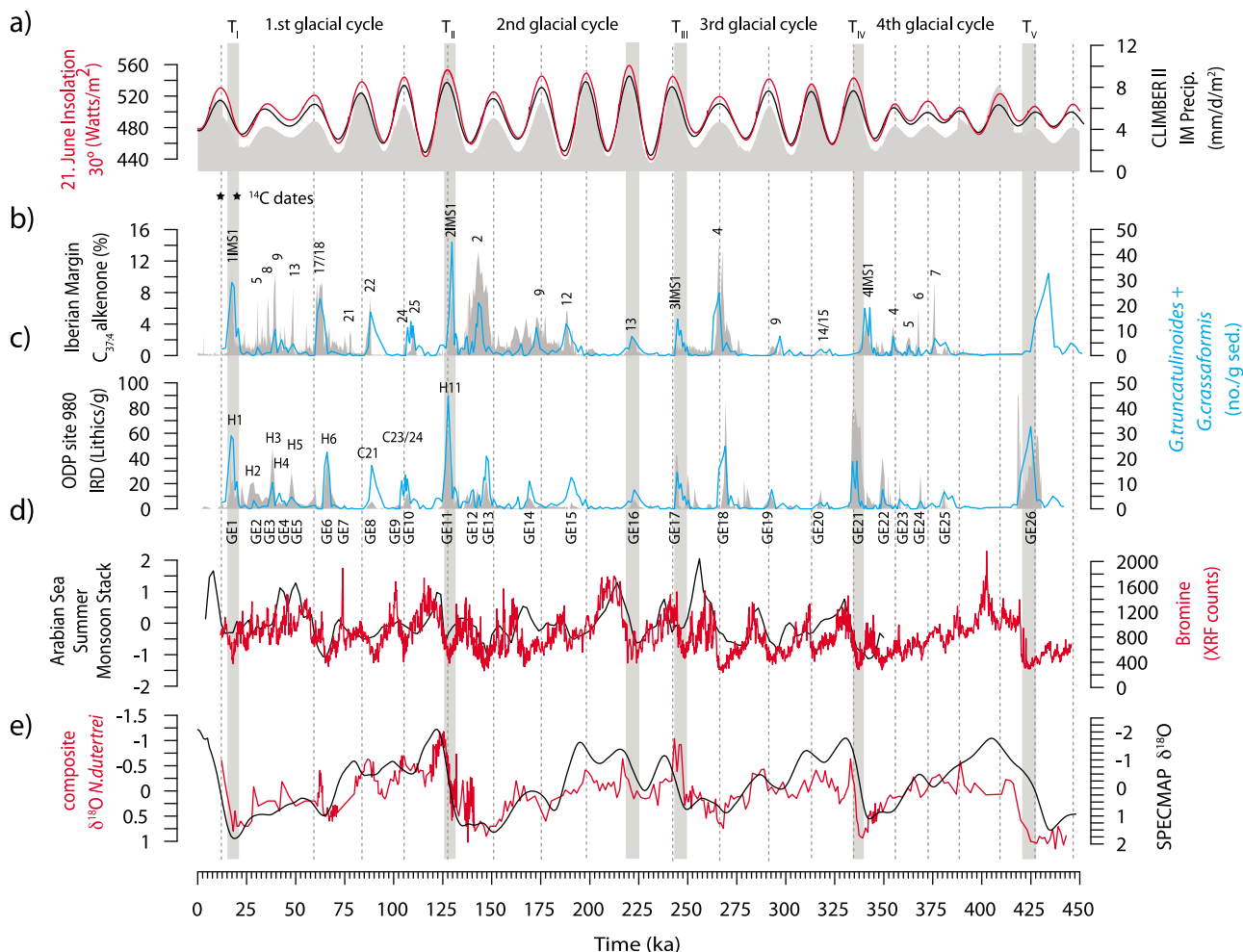


Figure 4. The Arabian Sea composite record plotted on the Iberian Margin-tied chronology and comparison with modeling results, astronomical insolation and other paleoclimate proxy data. (a) Summer (21 June) insolation at 30°N (black) and CLIMBER II modeled Indian Monsoon precipitation (red line, “orbital only” run; gray filled area, “orbital + ice-sheet run”). (b) Correlation of Arabian Sea *G. truncatulinoides* + *G. crassaformis* (*GE*) composite record (blue line) to Iberian margin record (MD01-2443/44) of relative proportion of tetraunsaturated C_{37} alkenone to total C_{37} alkenones ($C_{37:4}$), indicative of very cold surface waters at the core locations [Martrat et al., 2007]. Labels indicate Iberian Margin stadials. (c) Alignment of *GE* composite record (blue line) to North Atlantic IRD (%) record from ODP site 980 [McManus et al., 1999]. (d) Arabian Sea summer monsoon stack (SMS) [Clemens and Prell, 2003] (black line) and Arabian Sea Bromine composite record (red line; SPECMAP (ODP 980) age model). (e) Arabian Sea composite of planktic $\delta^{18}O$ (*N. dutertrei*) and SPECMAP $\delta^{18}O$ [Imbrie et al., 1984].

found at the 41-kyr (obliquity) and 100-kyr (i.e., glacial-interglacial scale) band (Figure 5b). This might be caused by a nonlinear relationship between North Atlantic and *GE* occurrences. In particular, relatively large *GE* peaks during interglacial periods correspond to relatively small North Atlantic cold events. The presence of a strong precession component is consistent with previous studies, which indicate that the abrupt cold events in the North Atlantic are precession paced [Chapman and Shackleton, 1998]. The Bromine power spectrum shows prominent peaks at 23, 40 and 91 kyr periods (Figure 5b). Blackman-Tukey cross-

spectral analysis for the time interval between 12 and 444 ka reveals that the 23-kyr component of the Bromine record lags June 21st insolation (30° N) - precession minima - with $128^\circ \pm 10^\circ$ or $\sim 7,900 \pm 600$ years (Figure 6a). For the 41-kyr obliquity component we estimated a phase lag of $58^\circ \pm 4^\circ$ or $\sim 6,400 \pm 450$ years. We repeated the cross-spectral analysis for the time interval between 12 and 224 ka, which revealed a much larger precession lag of $166^\circ \pm 20^\circ$ or $\sim 10,300 \pm 1,300$ years. Overall, the precession phase estimate based on the SPECMAP conform chronology is in general good agreement with the $\sim 124^\circ$ derived for the Arabian Sea

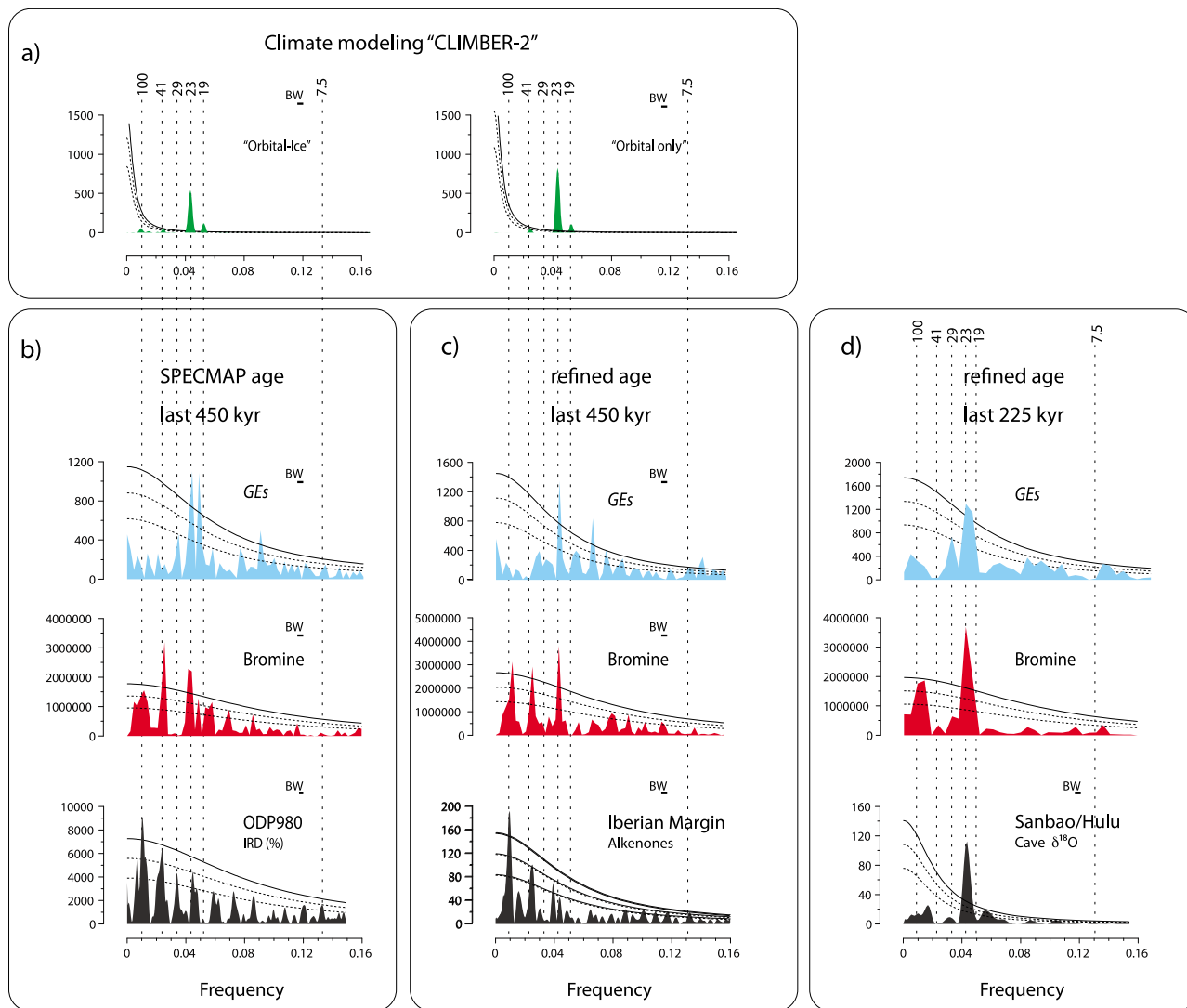


Figure 5. Power spectra calculated with the REDFIT-software [Schulz and Mudelsee, 2002]; red-noise boundaries were estimated as upper 80, 90 and 95% chi-square limits of a fitted AR1 process. Main periods are highlighted. (a) Power spectra of the CLIMBER-2 modeling results. (b) GE (blue) and Bromine (red) records on and IRD of ODP site 980 [McManus et al., 1999] (black) on SPECMAP conform age model for the interval 12–444 ka. (c) GE (blue) and Bromine (red) records on adapted age model for the interval 12–444 ka and Iberian Margin alkenones ($C_{37:4}$) [Martrat et al., 2007] (black). (d) GE (blue) and Bromine (red) records on adapted age model for the interval 12–224 ka and Sanbao-Hulu $\delta^{18}O$ [Wang et al., 2008] (black).

summer-monsoon stack [Clemens and Prell, 2003] and other studies [Altabet et al., 1999; Leuschner and Sirocko, 2003; Reichert et al., 1998; Schmiedl and Leuschner, 2005].

5.2. Refining the Chronology With Radioisotopic Age Constraints

[22] Having confirmed the long precession lag of the Arabian Sea productivity record, we will now test the hypothesis that this lag resulted from an overestimation of orbital phase-relations in the SPECMAP chronology. For this purpose we applied the tetraunsaturated to total C_{37}

alkenone-ratio ($C_{37:4}$) from the Portugal Margin cores MD01-2443/44 (Figure 3) [Martrat et al., 2007] as an alternative tuning target for the GEs (Figure 4b). The alkenone record reflects coldest temperatures at the core location and resembles IRD records from the North Atlantic. Its age model is largely based on tuning to Greenland and Antarctic records and is extremely well constrained by a large number radiocarbon dates during the last glacial cycle. To further refine our Iberian Margin based age model we considered U/Th-derived ages from speleothem records, which yield high-precision ages of North Atlantic cold events beyond the radiocarbon dates. The first age marker that we use originates

Table 3. GE and North Atlantic Cold Events, Corresponding Ages and Radioisotopic Age Constraints

<i>Globorotalia</i> Event	Composite Event (cm)	IRD Peaks ODP Site 980 (SPECMAP Age)	Iberian Margin Stadials	Age (Iberian Margin)	Additional Age Constraint Sources
GE1	17	17.1	Martrat1IMS2a	17.4	
GE2	137	28.5	Martrat1IMS6	30.6	
GE3	177	38.2	Martrat1IMS8	39.5	
GE4	259	47.9	Martrat1IMS9	48.6	
GE5	307	60.6	Martrat1IMS13	55.4	
GE6	358	67.0	Martrat1IMS17/18	62.8	H6 [<i>Genty et al.</i> , 2003] (61.2 ± 0.6 to 67.4 ± 0.9 ka)
GE7	435	74.7	Martrat1IMS21	77.7	
GE8	530	88.9	Martrat1IMS22	88.8	C 21 [<i>Wang et al.</i> , 2008] (85)
GE9	591	102.3	Martrat1IMS24	105.5	C 23 [<i>Drysdale et al.</i> , 2007] (105.1 ± 0.9 to 102.6 ± 0.8 ka)
GE10	673	107.0	Martrat1IMS25	110.8	C 24 [<i>Drysdale et al.</i> , 2007] (112.0 ± 0.8 to 108.8 ± 1.0 ka)
GE11	803	127.8	Martrat2IMS1	129.6	H11 [<i>Drysdale et al.</i> , 2005] (130 ± 2 ka)
GE12	922	140.7	Martrat2IMS2	137.4	Sanbao-Hulu (150)
GE13	1012	147.3	Martrat2IMS3	143.2	Sanbao-Hulu (158.2)
GE14	1242	169.2	Martrat2IMS9	172.7	Sanbao-Hulu (179.4)
GE15	1318.5	190.5	Martrat2IMS10	188.0	<i>Dutton et al.</i> [2009] (191)
GE16	1538.5	222.6	Martrat2IMS13	221.5	<i>Dutton et al.</i> [2009]/Sanbao monsoon minimum (225)
GE17	1691.5	244.6	Martrat3IMS1	244.8	<i>Dutton et al.</i> [2009] (250)
GE18	1941	269.2	Martrat3IMS4/5	266.0	
GE19	2101	292.6	Martrat3IMS9	296.9	
GE20	2229	318	Martrat3IMS13/14	318.0	
GE21	2396	335.6	Martrat4IMS1	342.4	
GE22	2658	349.4	Martrat4IMS4	354.8	
GE23	2725	358.1	Martrat4IMS5	362.8	
GE24	2800	368.8	Martrat4IMS6	367.7	
GE25	2864	380.7	Martrat4IMS7	375.9	
GE26	3078.5	425	TIRE5	434	

from a stalagmite in southwest France [*Genty et al.*, 2003]. The oxygen isotope record of this stalagmite shows an extreme cold phase from 61.2 ± 0.6 to 67.4 ± 0.9 ka which is associated with Heinrich 6 (Iberian Margin stadial 17/18). This U/Th age corresponds well with the age of the associated Iberian Margin stadial (61 to 63 ka) and but also with Heinrich 6 in ODP Site 980, which appears to be slightly older (66–68 ka). U/Th ages are also available for the C23 and C24 [*Chapman and Shackleton*, 1999] cold events (Iberian Margin stadials 24 and 25), as they are recorded in stalagmites located in the Italian Alps [*Drysdale et al.*, 2007]. The radioisotopic dates (C23: 102.6 ± 0.8 to 105.1 ± 0.9 ka and C24: and 108.8 ± 1.0 to 112.0 ± 0.8 ka) agree again well with ages of the corresponding Iberian Margin stadials (104.5–106 and 109–111), but show a small offset with ages of the corresponding IRD events in Site 980 (102–103.5 and 107–109). Another Italian stalagmite provides an U/Th age for an interruption of the penultimate deglaciation, which has been associated with Heinrich 11 [*Drysdale et al.*, 2005]: 130 ± 2 ka. The marine records yield slightly younger ages within the error margin: 127.8 (H11 in ODP Site 980) and 129.7 (2IMS1 in the Iberian Margin).

[23] Dated growth phases of stalagmites in a submerged cave (Argentarola) in Italy have recently provided accurate dates of sea level highstands during the penultimate interglacial (MIS7) [*Dutton et al.*, 2009]. We assigned the age that characterize the end of the sea level-highstand of MIS 7.1 at 189.7 ± 1.5 ka [*Dutton et al.*, 2009] to the Iberian margin stadial 2IMS10 (Figure 7). In addition, we used the onsets of MIS7.2 (217.2 ± 1.9 ka) and MIS7.3 (248.9 ± 1.9)

as ages for 2IMS13 and 3IMS1 (and their corresponding IRD events), respectively.

[24] In a last step of refining the age model we made use of the East Asian summer monsoon record from the Chinese Sanbao and Hulu Caves. Recently, the Asian monsoon speleothem record has been extended back to 224,000 years ago. The Hulu-Sanbao record is dated with 186 U/Th dates with an average dating error of less than 1% [*Wang et al.*, 2008, 2001]. Currently, it is the best-dated, high-resolution paleoclimate record covering the last two glacial cycles. Virtually identical fluctuations in the $\delta^{18}\text{O}$ record of independently dated individual stalagmites and the excellent agreement between records from Hulu [*Wang et al.*, 2001] and Dongge Cave [*Y. Wang et al.*, 2005] indicate the high-precision of the dating. It was previously shown in several studies, that the $\delta^{18}\text{O}$ record of the Hulu Cave correlates with Greenland stadial-interstadial variability on the millennial scale during the last glacial cycle [*Wang et al.*, 2001]. For comparison with our bromine record we constructed a $\delta^{18}\text{O}$ stack from selected stalagmites of the Sanbao-Hulu caves. We re-sampled the composite $\delta^{18}\text{O}$ records into 0.1 kyr increments using the *Analyseries* software [*Paillard et al.*, 1996]: SB3, SB10, SB11, SB22, SB23, SB25-1, SB26 from the Sanbao cave [*Wang et al.*, 2008] and MSD, MSL, YT, H82 from the Hulu cave [*Wang et al.*, 2001]. We used an average value per time interval for the stacked record.

[25] We note that the radioisotopically derived ages of North Atlantic cold events listed above fit all with maxima in the oxygen isotope record of the Sanbao-Hulu composite,

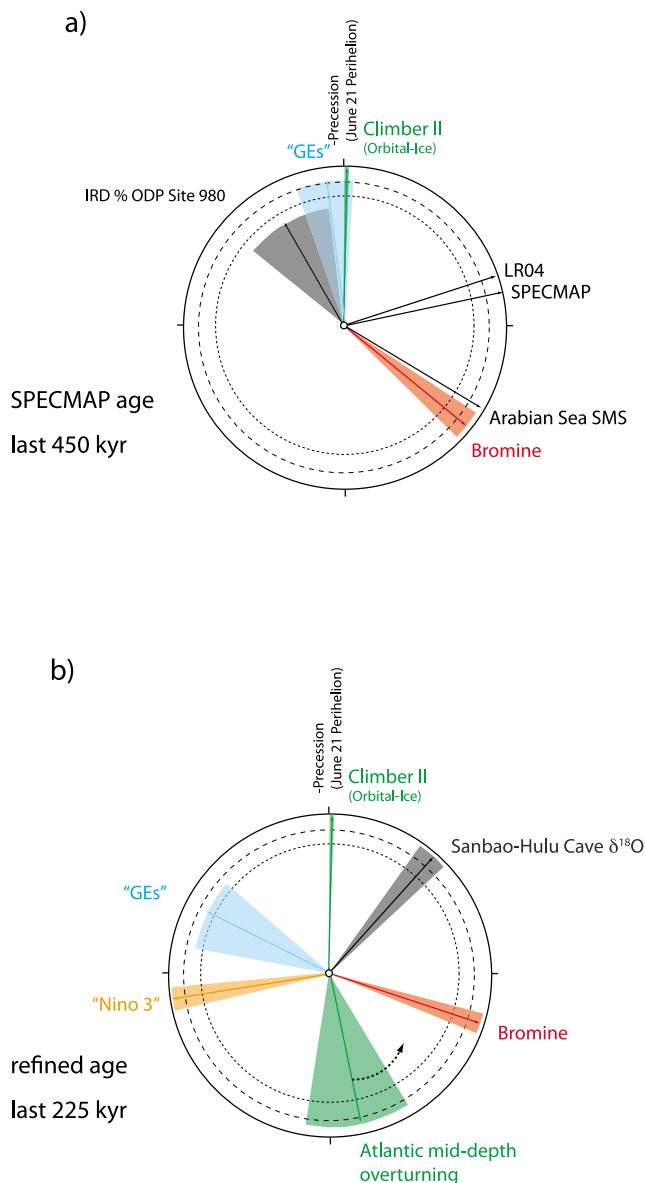


Figure 6. Phase wheels illustrating the phase relations between the different records at the precession band (23 kyr) (a) SPECMAP conform chronology (12–444 ka) and (b) adapted chronology (12–224 ka). In the phase wheel representation the 12 o'clock position is in phase with minimum precession (maximum summer insolation at the Northern Hemisphere). Phase lags increase in clockwise direction (3 o'clock equals 90° or 5.75 kyr phase lag). Vector length represents coherence (dotted circle marks 95%; dashed line marks 90%). Shaded areas represent 95% confidence interval of the phase estimate. Phase estimates and coherences were calculated with the Blackman-Tukey method using the *Analyseries* software.

thus confirming the close relationship between North Atlantic cold events and summer monsoon minima. Similarly, North Atlantic cold event C21 is recognizable as an interruption of a period of strong summer monsoon at

86.8 ka (Figure 7). In that respect it seems odd that the extreme Iberian margin stadial 2IMS2-3 and the corresponding IRD event in Site 980 coincide with a monsoon maximum in the Sanbao record. We therefore followed the Sanbao age model and decided to shift 2IMS2 to 2IMS9 approximately 10 kyr older (Table 1).

[26] Subsequently, we adjusted the ages of the *GEs* in the Arabian Sea using the new radioisotopic age constraints and recapitulated the precession phase of the Bromine record. As a result, we now find that Bromine maxima lag precession minima by $95^\circ \pm 6^\circ$ or $\sim 6,000 \pm 400$ years for the interval between 12 and 444 ka (Figure 6b). For the 41-kyr obliquity component we estimated a phase lag of $30^\circ \pm 6^\circ$ or $\sim 3,400 \pm 650$ years. In addition, cross-spectral analysis for the 12 to 224 ka, revealed a slightly larger precession lag of $109^\circ \pm 3^\circ$ or $\sim 6,900 \pm 200$ years (Figure 6b). Our results clearly imply that an offset in the SPECMAP chronology cannot entirely explain the long precession phase found in the Arabian Sea productivity records. Application of radioisotopic age constraints to refine the age model shows that the chronology could explain up to 2,000 or 3,000 years of the total time lag. Indeed it has been suggested, based on independent age constraints on the timing of the penultimate glacial termination, that the response times in the SPECMAP chronology are overestimated [Gallup *et al.*, 2002; Henderson and Slowey, 2000; Spötl *et al.*, 2002]. However, the uncertainties involved in the construction of the age model, do not allow a revision of the SPECMAP phase lags yet.

6. Discussion

6.1. Comparison With Sanbao-Hulu Summer Monsoon Record

[27] The precession lag of the summer monsoon as recorded in the Chinese Sanbao and Hulu caves speleothem record is $\sim 2,700$ years (Figure 6b) and thus 3,000 to 4,000 years shorter than the time lag derived from our Arabian Sea productivity record on the refined timescale. The short time lag of the speleothem record is consistent with the adopted precession phasing of Late Pleistocene Mediterranean sapropel layers of 3 kyr [Lourens *et al.*, 1996; Lourens, 2004], which are related to maximum intensity of the African Monsoon [Rossignol-Strick, 1983]. Moreover, it agrees well with the 2.6 kyr time lag of atmospheric methane concentrations recorded in an ice core from Antarctica [Loulergue *et al.*, 2008; Spahni *et al.*, 2005]. Atmospheric methane is largely related to the extent of tropical wetlands thus providing an integrated global monsoon signal. Although the shorter time lag is in general good agreement with our modeling results, the $\sim 2,700$ year time lag suggests that our climate model experiments lack important feedback mechanisms, such as the imprint of rapid, sub-Milankovitch climate changes. Indeed, other investigations with the CLIMBER-2 model showed that freshwater pulses into the North Atlantic weakened the African and Asian monsoon [Jin *et al.*, 2007; Tjallingii *et al.*, 2008]. In a separate paper, we adopted these findings in a conceptual model and found that precession-paced North Atlantic cold events could produce the small phase

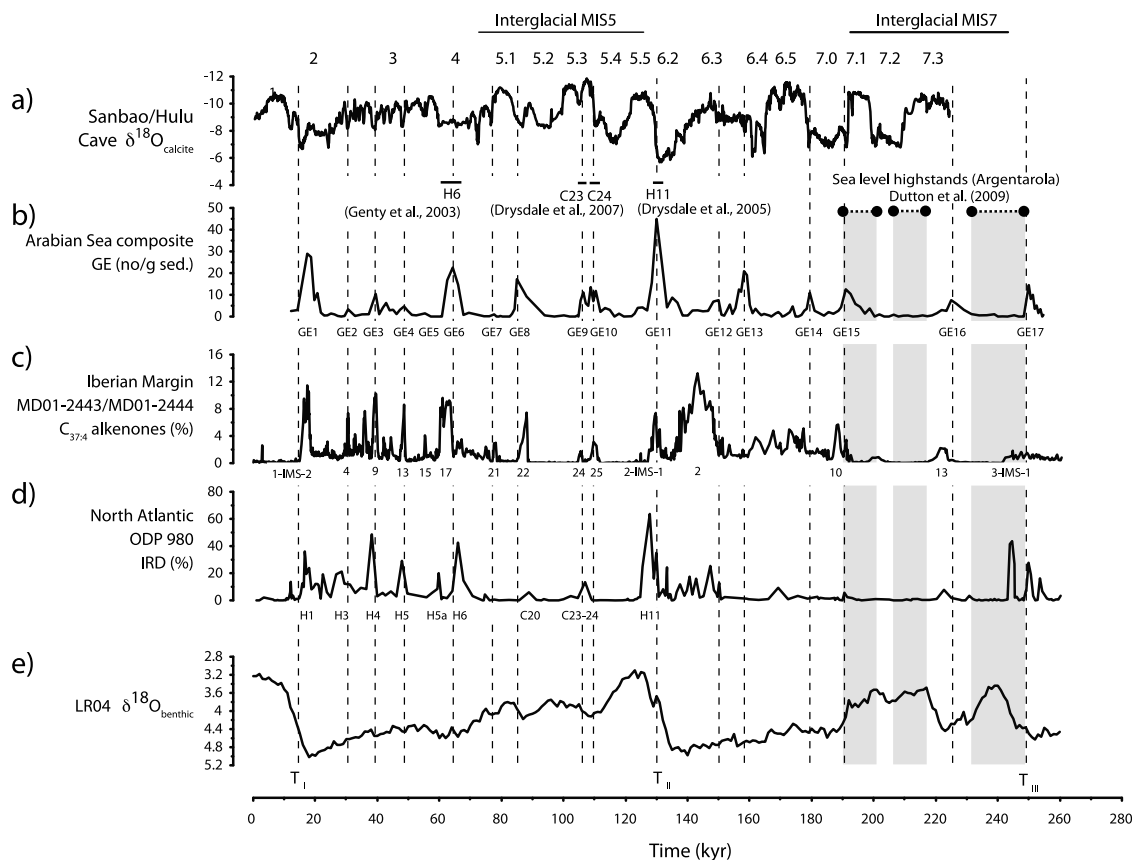


Figure 7. (a) Sanbao/Hulu cave $\delta^{18}\text{O}$ [Wang et al., 2008]. (b) GE record Arabian Sea (with GE numbering) on revised chronology. (c) Iberian Margin alkenones ($\text{C}_{37:4}$) [Martrat et al., 2007] (with IMS numbering). (d) North Atlantic IRD record from ODP site 980 [McManus et al., 1999]. (e) Global benthic oxygen isotope stack LR04 [Lisiecki and Raymo, 2005]. Stippled lines indicate age control points for the adapted chronology, based on radioisotopic ages.

lag in the Chinese speleothem as well as in the Mediterranean sapropel record [Ziegler et al., 2010a].

[28] Initially, we expected that changes in northern Arabian Sea productivity and OMZ intensity would portray a similar $\sim 2,700$ years time lag, because millennial-scale, Dansgaard-Oeschger-type variability in the speleothem $\delta^{18}\text{O}$ record [Wang et al., 2008] can also be identified in the Bromine record; i.e., conform earlier high-resolution studies of the Arabian Sea [Altabet et al., 2002; Schulz et al., 1998]. Moreover, the sharp increase in summer monsoon intensity associated with the timing of glacial termination T_{II} in the Chinese speleothem record is closely aligned with the productivity and OMZ intensity increase in the Arabian Sea. In fact, initially we tuned the precession signal in the Bromine record to that in the speleothem $\delta^{18}\text{O}$ record in order to establish a refined chronology for the GEs and hence the cold water events in the North Atlantic. This approach led however to such large offsets between current U/Th dated sea level constraints and the resulting global benthic $\delta^{18}\text{O}$ record that we refrained from discussing this option here.

[29] Hence, we conclude that the mismatch between the Bromine and speleothem $\delta^{18}\text{O}$ record most likely indicates that primary productivity in the Arabian Sea and summer

monsoon intensity are decoupled at the precession frequency. Such a decoupling excludes theories which invoke a maximum latent heat transport during southern hemisphere insolation maxima [Clemens et al., 1991; Clemens and Prell, 2003], because these infer a direct coupling between summer monsoon intensities and upwelling driven productivity changes in the Arabian Sea. It may be important to note that the summer monsoon stack of Clemens and Prell [2003] actually represents a productivity stack, as four out of the five proxies used are linked to productivity. The only exception is the lithogenic grain-size proxy, which was interpreted as a wind-strength indicator. However, it can be argued that grain-size also depends on the vegetation coverage in the dust source area [Clemens and Prell, 2003]. This may explain why the grain-size record of the Arabian Sea shows a distinct minimum during the Holocene, whereas the “productivity-stack” indicates a large maximum [Clemens and Prell, 2003]. Similarly, a comparison between $\delta^{15}\text{N}$ and a lithogenic grain size record from the Arabian Sea over the last 1 million years [Altabet et al., 1999] shows many of such mismatches. We argue that grain size records do not represent wind strength only, because not only vegetation in the source area, but also additional influences

such as e.g., distance to the dust source or available material at the source may play an important role. *Malaizé et al.* [2006] suggested a temporal decoupling between summer monsoon precipitation and wind strength across the Arabian Sea related to the position of the ITCZ. We propose an alternative mechanism, which builds on results from ocean modeling.

6.2. Changes in the AMOC and Arabian Sea Productivity Conditions

[30] A detailed, three-dimensional ocean simulation of export production and oxygen and nitrogen cycling during idealized Dansgaard-Oeschger cycles demonstrated that the millennial-scale variability, which can be observed in Arabian Sea OMZ-intensity and paleoproductivity records, can be explained by oceanographic changes rather than atmospheric processes [*Schmittner*, 2005; *Schmittner et al.*, 2007]. *Schmittner et al.* [2007] demonstrated that nutrient availability, primary productivity and the intensity of the OMZ in the northern Indian Ocean are all highly sensitive to the strength of the AMOC with only little time lag (200–400 years) between AMOC changes and shifts in oxygenation levels of the Arabian Sea. In the model, reduced NADW formation leads to a dramatic decrease in the interbasin difference in deep water oxygen concentrations. Whereas, oxygen concentrations decrease in Atlantic deep waters, they increase in the Indo-Pacific surface waters. At the same time the reduced export of nutrient-rich waters to the Indian and Pacific euphotic zones leads to a decline of the export production. A combination of both factors is sufficient to explain the millennial scale variability in the Arabian Sea sediment records. According to their modeling results changes in wind-driven upwelling represent a secondary source of variability only.

[31] Because AMOC varies also on the Milankovitch-scale [*Lisiecki et al.*, 2008; *Imbrie et al.*, 1992], one can expect that the oceanographic processes described above will affect the nutrient balance in the Arabian Sea on these longer timescales as well. *Lisiecki et al.* [2008] derived an anti-phase relationship (170° lag) between maxima in the AMOC and northern hemisphere summer insolation in the precession frequency band based on benthic foraminifera $\delta^{13}\text{C}$ records of the Atlantic and Pacific [*Lisiecki et al.*, 2008]. Their underlying chronology, LR04 [*Lisiecki and Raymo*, 2005], applies similar phase lags as the SPECMAP model. Based on our refined age model, this would imply that the precession lag in the overturning circulation should also become ~2,500 years shorter and thus close to the lag that we derive for maximized productivity conditions in the Arabian Sea (indicated by black stippled arrow in Figure 6b). In analog to the results of *Schmittner et al.* [2007], the almost similar precession lag of AMOC [*Lisiecki et al.*, 2008] and Arabian Sea OMZ maxima implies that the precession phase of the Arabian Sea proxy records are dominated by AMOC variability rather than Monsoon variability.

[32] This proposed mechanism implies that minimum AMOC at the precession scale occurs roughly synchronous with *Globorotalia* ventilation events in the Arabian Sea, and is thus coupled with to North Atlantic cold events when deep water formation in the North Atlantic ceased [*Rahmstorf*, 2002]. Indeed, *Ziegler et al.* [2010a] showed

that the timing of these North Atlantic cold events is paced by the precession cycle, and argued that these events postponed monsoon intensification at the onset of NH summer warming, resulting in the small precession lag of ~3 kyrs as found in the Mediterranean sapropel record and Chinese speleothem monsoon-records. All this suggests that the North Atlantic cold events not only weakened the summer monsoon, the primary driver of upwelling in the Arabian Sea, but also reduced the AMOC which reduced nutrient supply to the Arabian Sea surface hence reducing export production there. In this light, the extreme high productivity conditions in the Arabian Sea during marine isotope stage 13 has also been explained by a similar combination of oceanic (AMOC) and atmospheric (Monsoon) processes rather than atmospheric forcing alone [*Ziegler et al.*, 2010b].

6.3. Potential Links to Orbital-Controlled ENSO Variations

[33] Earlier studies have proposed linkages between Indian Ocean productivity changes and the El Niño-Southern Oscillation (ENSO) on orbital timescales. *Beaufort et al.* [2001] suggested a direct coupling between precession-controlled equatorial paleo-productivity (ePP) variations and ENSO related changes in the east-west thermocline slope of the Indo-Pacific, notwithstanding an average phase shift of ~5 kyr found between the modeled NINO3 index [*Clement and Cane*, 1999] and the ePP records derived from the central Indian Ocean and the western and eastern Pacific. A comparison between the modeled NINO3 index [*Clement and Cane*, 1999] and our Bromine minima reveal on the other hand a very good fit (Figure 8) and therefore an opposite precession phase (Figure 6) over the past 225,000 years. This suggests that the OMZ and productivity minima and hence AMOC minima occur during periods of more frequent El Niño events. In view of these similar phase relations, we conjecture that ENSO, AMOC and productivity and OMZ variability in the Arabian Sea are linked on precessional timescales. This may imply that ENSO-related processes are indirectly, through changes in AMOC, responsible for the exceptionally long precession phase of the productivity and OMZ variations in the Arabian Sea. In turn, such an explanation is in good agreement with the synchronous behavior of summer monsoon intensity, Arabian Sea primary productivity, North Atlantic temperatures and Super-ENSOs on millennial time scales [*Stott et al.*, 2002; *Turney et al.*, 2004; *Wang et al.*, 2001].

[34] Finally, more sophisticated, higher resolution, transient Earth System modeling will be necessary to test our hypothesis. We also note, that our line of reasoning does not explain the long precession lags in South China Sea SST [*Chen et al.*, 2003] and Japanese pollen records [*Morley and Heusser*, 1997; *Igarashi and Oba*, 2006], which have been interpreted as summer monsoon strength indicators as well. Explaining those results remains also to be solved in future studies.

7. Conclusions

[35] We present a new high-resolution record of primary productivity and OMZ variability in the northern Arabian

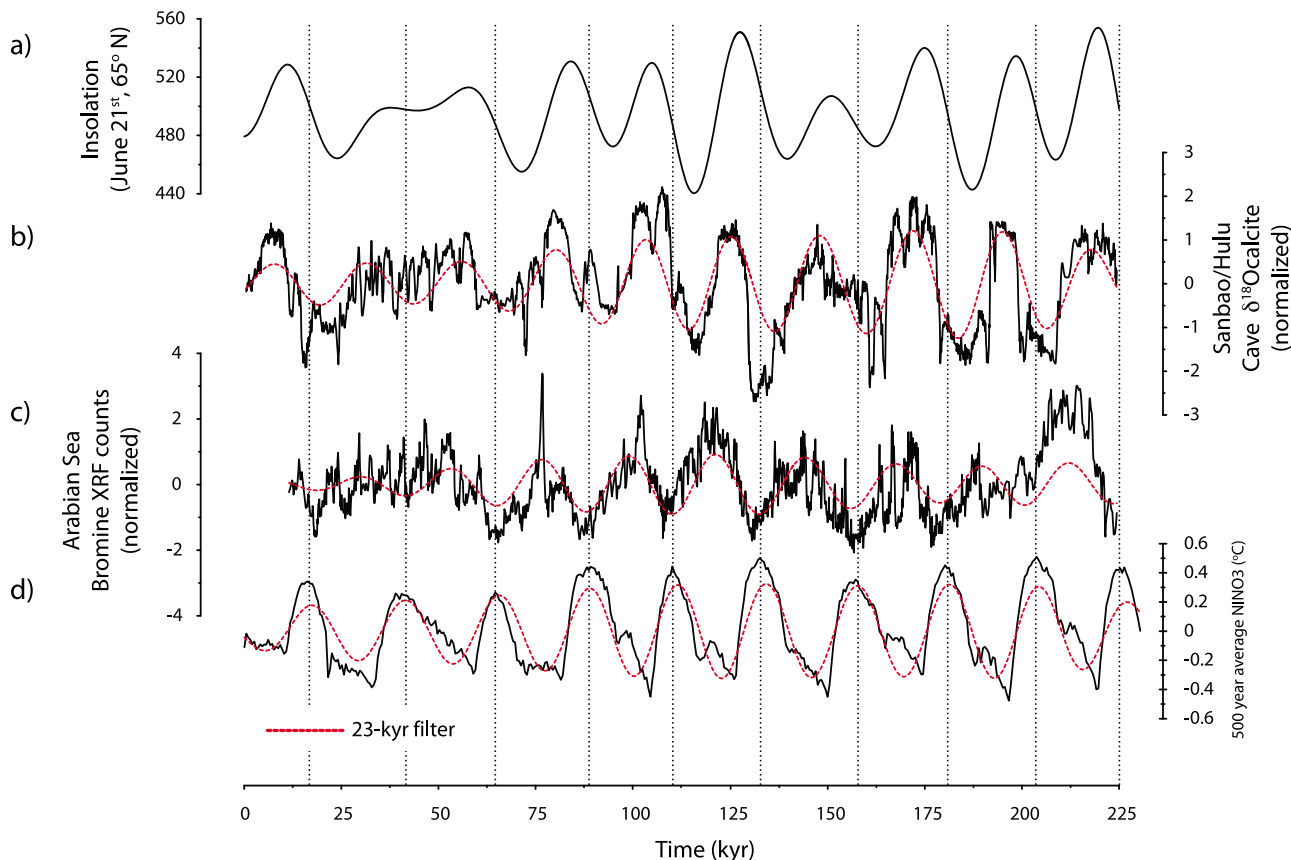


Figure 8. (a) Insolation, June 21st, 65°N. (b) Sanbao/Hulu cave $\delta^{18}\text{O}$ [Wang et al., 2008]. (c) Arabian Sea Bromine record on adapted chronology. (d) Modeled NINO3 500 year average [Clement and Cane, 1999]. Red stippled lines are 23-kyr Gaussian filters.

Sea over the last 444,000 years. Cross-spectral results indicate a 6,000–7,000 years lag relative to precession minima that is consistent with previous studies. We therefore conclude that the established precession phase relation for primary productivity and OMZ variability in the northern Arabian Sea is robust, notwithstanding the different proxies applied in the literature. This also seems to rule out that the lag is an artifact due to secondary effects (e.g., preservation). Our oxygen isotope tuning-independent age model further indicates that the observed precession phase is not related to the potential diachronous nature of oxygen isotope variations between different ocean basins. New transient climate modeling results indicate that glacial-interglacial ice volume variations have no large impact on the precession phasing of the monsoon and instead confirm the earlier found (almost) in-phase relationship between precession minima and summer monsoon maxima. However, these modeling experiments are still relatively simple and need to be improved in the future. For instance, the inability of the model to produce the small precession lag which is found in independent monsoon archives (i.e., Chinese stalagmite records and atmospheric methane in Antarctic ice cores) indicates that important feedback

mechanisms are missing in our model of intermediate complexity, such as the effect of North Atlantic cold events on the monsoon. We have tested the hypothesis that the large monsoon time lag is related to overestimated response times in the underlying marine isotope chronology (i.e., SPECMAP) by independent radioisotopic constraints. From these results we conclude that uncertainties in the SPECMAP chronology may lead to an overestimation of the precession time lag of $\sim 2,000$ years. Based on the comparison between the U/Th dated Chinese speleothem $\delta^{18}\text{O}$ record and our reconstructed productivity and OMZ record of the Arabian Sea, we conclude that Arabian Sea primary productivity and OMZ intensity are decoupled from Asian summer monsoon strength on precessional time scales. The precession phase of Arabian Sea productivity much rather seems to be controlled by variations in AMOC as a reduction in AMOC, which leads precession maxima by 3,000 years, will limit nutrient supply to the Arabian Sea surface waters and increase oxygenation of the Indian Ocean subsurface.

[36] **Acknowledgments.** This study is supported by the Research Council for Earth and Life Sciences (ALW) with financial aid from the

Netherlands Organization for Scientific Research (NWO) to L. J. Lourens (grants 853.00.032 and 834.04.003). We thank the reviewers Luc Beaufort and Steven Clemens and editors Jerry Dickens and Rainer Zahn for their

thoughtful comments. H. Abels, A. van Dijk, R. Giles, G. Ittman, T. Jilbert, K. Koho, T. Richter, and A. Vaars are thanked for discussion and technical support.

References

- Altabet, M. A., D. W. Murray, and W. L. Prell (1999), Climatically linked oscillations in Arabian Sea denitrification over the past 1 m.y.: Implications for the marine N cycle, *Paleoceanography*, *14*, 732–743, doi:10.1029/1999PA900035.
- Altabet, M. A., M. J. Higginson, and D. W. Murray (2002), The effect of millennial-scale changes in Arabian Sea denitrification on atmospheric CO₂, *Nature*, *415*, 159–162, doi:10.1038/415159a.
- Antoine, D., J.-M. André, and A. Morel (1996), Oceanic primary production: 2. Estimation at global scale from satellite (coastal zone color scanner) chlorophyll, *Global Biogeochem. Cycles*, *10*(1), 57–69, doi:10.1029/95GB02832.
- Beaufort, L., T. de Garidel-Thoron, A. C. Mix, and N. G. Pisias (2001), ENSO-like forcing on oceanic primary production during the Late Pleistocene, *Science*, *293*(5539), 2440–2444, doi:10.1126/science.293.5539.2440.
- Bintanja, R., R. S. W. van de Waal, and J. Oerlemans (2005), Modelled atmospheric temperatures and global sea levels over the past million years, *Nature*, *437*, 125–128, doi:10.1038/nature03975.
- Calov, R., A. Ganopolski, V. Petoukhov, M. Claussen, V. Brovkin, and C. Kubatzki (2005), Transient simulation of the last glacial inception. Part II: Sensitivity and feedback analysis, *Clim. Dyn.*, *24*, 563–576.
- Chapman, M. R., and N. J. Shackleton (1998), Millennial-scale fluctuations in North Atlantic heat flux during the last 150,000 years, *Earth Planet. Sci. Lett.*, *159*, 57–70, doi:10.1016/S0012-821X(98)00068-5.
- Chapman, M. R., and N. J. Shackleton (1999), Global ice-volume fluctuations, North Atlantic ice-rafting events, and deep-ocean circulation changes between 130 and 70 ka, *Geology*, *27*(9), 795–798, doi:10.1130/0091-7613(1999)027<0795:GIVFNA>2.3.CO;2.
- Chen, M.-T., L.-J. Shiau, P.-S. Yu, T.-C. Chiu, Y.-G. Chen, and K.-Y. Wei (2003), 500 000-year records of carbonate, organic carbon, and foraminiferal sea-surface temperature from the southeastern South China Sea (near Palawan Island), *Palaeogeogr. Palaeoclimatol. Palaeoecol.*, *197*, 113–131, doi:10.1016/S0031-0182(03)00389-4.
- Clemens, S. C., and W. L. Prell (2003), A 350,000 year summer-monsoon multi-proxy stack from the Owen Ridge, northern Arabian Sea, *Mar. Geol.*, *201*(1–3), 35–51, doi:10.1016/S0025-3227(03)00207-X.
- Clemens, S., W. Prell, D. Murray, G. Shimmield, and G. Weedon (1991), Forcing mechanisms of the Indian Ocean monsoon, *Nature*, *353*, 720–725, doi:10.1038/353720a0.
- Clemens, S. C., D. W. Murray, and W. L. Prell (1996), Nonstationary phase of the Pliocene-Pleistocene Asian monsoon, *Science*, *274*(5289), 943–948, doi:10.1126/science.274.5289.943.
- Clement, A. C., and M. Cane (1999), A role for the tropical Pacific coupled ocean-atmosphere system on Milankovitch and millennial time-scales. Part I: A modeling study of tropical Pacific variability, in *Mechanisms of Global Climate Change at Millennial Time Scales*, *Geophys. Monogr. Ser.*, vol. 112, edited by P. U. Clark, R. S. Webb, and L. D. Keigwin, pp. 363–372, AGU, Washington, D. C.
- den Dulk, M., G. J. Reichert, S. van Heyst, W. J. Zachariasse, and G. J. Van der Zwaan (2000), Benthic foraminifera as proxies of organic matter flux and bottom water oxygenation? A case history from the northern Arabian Sea, *Palaeogeogr. Palaeoclimatol. Palaeoecol.*, *161*, 337–359, doi:10.1016/S0031-0182(00)00074-2.
- Drysdale, R. N., G. Zanchetta, J. C. Hellstrom, A. E. Fallick, and J. Zhao (2005), Stalagmite evidence for the onset of the last interglacial in southern Europe at 129 ± 1 ka, *Geophys. Res. Lett.*, *32*, L24708, doi:10.1029/2005GL024658.
- Drysdale, R. N., G. Zanchetta, J. C. Hellstrom, A. E. Fallick, J. McDonald, and I. Cartwright (2007), Stalagmite evidence for the precise timing of North Atlantic cold events during the early last glacial, *Geology*, *35*(1), 77–80, doi:10.1130/G23161A.1.
- Dutton, A., E. Bard, F. Antonioli, T. M. Esat, K. Lambeck, and M. T. McCulloch (2009), Phasing and amplitude of sea-level and climate change during the penultimate interglacial, *Nat. Geosci.*, *2*, 355–359, doi:10.1038/ngeo470.
- Gallup, C. D., H. Cheng, F. W. Taylor, and R. L. Edwards (2002), Direct determination of the timing of sea level change during Termination II, *Science*, *295*(5553), 310–313, doi:10.1126/science.1065494.
- Ganopolski, A., S. Rahmstorf, V. Petoukhov, and M. Claussen (1998a), Simulation of modern and glacial climates with a coupled global model of intermediate complexity, *Nature*, *391*, 351–356.
- Ganopolski, A., C. Kubatzki, M. Claussen, V. Brovkin, and V. Petoukhov (1998b), The influence of vegetation-atmosphere-ocean interaction on climate during the Mid-Holocene, *Science*, *280*(5371), 1916–1919.
- Ganopolski, A., V. Petoukhov, S. Rahmstorf, V. Brovkin, M. Claussen, A. Eliseev, and C. Kubatzki (2001), CLIMBER-2: A climate system model of intermediate complexity. Part II—Model sensitivity, *Clim. Dyn.*, *17*, 735–751, doi:10.1007/s003820000144.
- Genty, D., D. Blamart, R. Ouahdi, M. Gilmour, A. Baker, J. Jouzel, and S. Van-Exer (2003), Precise dating of Dansgaard-Oeschger climate oscillations in western Europe from stalagmite data, *Nature*, *421*, 833–837, doi:10.1038/nature01391.
- Gupta, A. K., M. Das, S. C. Clemens, and B. Mukherjee (2008), Benthic foraminiferal faunal and isotopic changes as recorded in Holocene sediments of the northwest Indian Ocean, *Paleoceanography*, *23*, PA2214, doi:10.1029/2007PA001546.
- Henderson, G. M., and N. C. Slowey (2000), Evidence from U-Th dating against Northern Hemisphere forcing of the penultimate deglaciation, *Nature*, *404*, 61–66, doi:10.1038/35003541.
- Huguet, C., J.-H. Kim, J. S. Sinninghe Damsté, and S. Schouten (2006), Reconstruction of sea surface temperature variations in the Arabian Sea over the last 23 kyr using organic proxies (TEX₈₆ and U₃₇^K), *Paleoceanography*, *21*, PA3003, doi:10.1029/2005PA001215.
- Igarashi, Y., and T. Oba (2006), Fluctuations in the East Asian monsoon over the last 144 ka in the northwest Pacific based on a high-resolution pollen analysis of IMAGES core MD01-2421, *Quat. Sci. Rev.*, *25*, 1447–1459, doi:10.1016/j.quascirev.2005.11.011.
- Imbrie, J., J. D. Hays, D. G. Martinson, A. McIntyre, A. C. Mix, J. J. Morley, N. G. Pisias, W. L. Prell, and N. J. Shackleton (1984), The orbital theory of Pleistocene climate: Support from a revised chronology of the marine δ¹⁸O record, in *Milankovitch and Climate: Part I*, edited by A. Berger, pp. 269–305, D. Reidel, Dordrecht, Netherlands.
- Imbrie, J., et al. (1992), On the structure and origin of major glaciation cycles: 1. Linear responses to Milankovitch forcing, *Paleoceanography*, *7*, 701–738.
- Imbrie, J., et al. (1993), On the structure and origin of major glaciation cycles: 2. The 100,000-year cycle, *Paleoceanography*, *8*, 699–735, doi:10.1029/93PA02751.
- Jaeschke, A., M. Ziegler, E. C. Hopmans, G.-J. Reichert, L. J. Lourens, S. Schouten, and J. S. Sinninghe Damsté (2009), Molecular fossil evidence for anaerobic ammonium oxidation in the Arabian Sea over the last glacial cycle, *Paleoceanography*, *24*, PA2202, doi:10.1029/2008PA001712.
- Jin, L., F. Chen, A. Ganopolski, and M. Claussen (2007), Response of East Asian climate to Dansgaard/Oeschger and Heinrich events in a coupled model of intermediate complexity, *J. Geophys. Res.*, *112*, D06117, doi:10.1029/2006JD007316.
- Jung, S. J. A., G. M. Ganssen, and G. R. Davies (2001), Multidecadal variations in the early Holocene outflow of Red Sea water into the Arabian Sea, *Paleoceanography*, *16*, 658–668, doi:10.1029/2000PA000592.
- Kutzbach, J. E., X. Liu, Z. Liu, and C. Chen (2008), Simulation of the evolutionary response of global summer monsoons to orbital forcing over the past 280,000 years, *Clim. Dyn.*, *30*, 567–579, doi:10.1007/s00382-007-0308-z.
- Leuschner, D. C., and F. Sirocco (2003), Orbital insolation forcing of the Indian Monsoon—A motor for global climate changes?, *Palaeogeogr. Palaeoclimatol. Palaeoecol.*, *197*, 83–95, doi:10.1016/S0031-0182(03)00387-0.
- Lisiecki, L. E., and M. E. Raymo (2005), A Pliocene-Pleistocene stack of 57 globally distributed benthic δ¹⁸O records, *Paleoceanography*, *20*, PA1003, doi:10.1029/2004PA001071.
- Lisiecki, L. E., and M. E. Raymo (2009), Diachronous benthic δ¹⁸O responses during late Pleistocene terminations, *Paleoceanography*, *24*, PA3210, doi:10.1029/2009PA001732.
- Lisiecki, L. E., M. E. Raymo, and W. B. Curry (2008), Atlantic overturning responses to Late Pleistocene climate forcings, *Nature*, *456*, 85–88, doi:10.1038/nature07425.
- Locarnini, R. A., A. V. Mishonov, J. I. Antonov, T. P. Boyer, and H. E. Garcia (2006), *World Ocean Atlas 2005*, vol. 1, *Temperature*, NOAA Atlas NESDIS, vol. 61, edited by S. Levitus, 182 pp., NOAA, Silver Spring, Md.

- Loulergue, L., A. Schilt, R. Spahni, V. Masson-Delmotte, T. Blunier, B. Lemieux, J.-M. Barnola, D. Raynaud, T. F. Stocker, and J. Chappellaz (2008), Orbital and millennial-scale features of atmospheric CH₄ over the past 800,000 years, *Nature*, *453*, 383–386, doi:10.1038/nature06950.
- Lourens, L. J. (2004), Revised tuning of Ocean Drilling Program Site 964 and KC01B (Mediterranean) and implications for the δ¹⁸O, tephra, calcareous nannofossil, and geomagnetic reversal chronologies of the past 1.1 Myr, *Paleoceanography*, *19*, PA3010, doi:10.1029/2003PA000997.
- Lourens, L. J., A. Antonarakou, F. J. Hilgen, A. A. M. Van Hoof, C. Vergnaud-Grazzini, and W. J. Zachariasse (1996), Evaluation of the Plio-Pleistocene astronomical time-scale, *Paleoceanography*, *11*, 391–413, doi:10.1029/96PA02691.
- Malaizé, B., C. Joly, M.-T. Vénec-Peyré, F. Bassinot, N. Caillon, and K. Charlier (2006), Phase lag between Intertropical Convergence Zone migration and subtropical monsoon onset over the northwestern Indian Ocean during marine isotopic substage 6.5 (MIS 6.5), *Geochem. Geophys. Geosyst.*, *7*, Q12N08, doi:10.1029/2006GC001353.
- Martinson, D. G. (1987), Age dating and the orbital theory of the ice ages: Development of a high-resolution 0 to 300,000 year chronostratigraphy, *Quat. Res.*, *27*, 1–29, doi:10.1016/0033-5894(87)90046-9.
- Martrat, B., J. O. Grimalt, N. J. Shackleton, L. de Abreu, M. A. Hutterli, and T. F. Stocker (2007), Four climate cycles of recurring deep and surface water destabilizations on the Iberian Margin, *Science*, *317*(5837), 502–507, doi:10.1126/science.1139994.
- McManus, J. F., D. W. Oppo, and J. L. Cullen (1999), A 0.5-million-year record of millennial-scale climate variability in the North Atlantic, *Science*, *283*(5404), 971–975, doi:10.1126/science.283.5404.971.
- Morley, J. J., and L. E. Heusser (1997), Role of orbital forcing in East Asian monsoon climates during the last 350 kyr: Evidence from terrestrial and marine climate proxies from core RC14-99, *Paleoceanography*, *12*, 483–493, doi:10.1029/97PA00213.
- Paillard, D., L. Labeyrie, and P. Yiou (1996), Macintosh program performs time-series analysis, *Eos Trans. AGU*, *77*(39), 379, doi:10.1029/96EO00259.
- Peltier, W. R. (2004), Global glacial isostasy and the surface of the ice-age Earth: The ICE-5G (VM2) model and GRACE, *Annu. Rev. Earth Planet. Sci.*, *32*, 111–149, doi:10.1146/annurev.earth.32.082503.144359.
- Petoukhov, V., A. Ganopolski, V. Brovkin, M. Claussen, A. Eliseev, C. Kubatzki, and S. Rahmstorf (2000), CLIMBER-2: A climate system model of intermediate complexity. Part I—Model description and performance for present climate, *Clim. Dyn.*, *16*, 1–17, doi:10.1007/PL00007919.
- Rahmstorf, S. (2002), Ocean circulation and climate during the past 120,000 years, *Nature*, *419*, 207–214, doi:10.1038/nature01090.
- Reichart, G. J., L. J. Lourens, and W. J. Zachariasse (1998), Temporal variability in the northern Arabian Sea oxygen minimum zone (OMZ) during the last 225,000 years, *Paleoceanography*, *13*, 607–621, doi:10.1029/98PA02203.
- Reichart, G.-J., H. Brinkhuis, F. Huiskamp, and W. J. Zachariasse (2004), Hyperstratification following glacial overturning events in the northern Arabian Sea, *Paleoceanography*, *19*, PA2013, doi:10.1029/2003PA000900.
- Richter, T. O., S. van der Gaast, B. Koster, A. Vaars, R. Gieles, H. C. de Stigter, H. de Haas, T. C. E. van Weering, and R. G. Rothwell (2006), The Avaatech XRF Core Scanner: Technical description and applications to NE Atlantic sediments, in *New Techniques in Sediment Core Analysis*, edited by R. G. Rothwell, *Geol. Soc. Spec. Publ.*, *267*, 39–50.
- Rosignol-Strick, M. (1983), African monsoons, an immediate climatic response to orbital insolation, *Nature*, *304*, 46–49, doi:10.1038/304046a0.
- Ruddiman, W. F. (2006), What is the timing of orbital-scale monsoon changes?, *Quat. Sci. Rev.*, *25*, 657–658, doi:10.1016/j.quascirev.2006.02.004.
- Saher, M. H., F. Rostek, S. J. A. Jung, E. Bard, R. R. Schneider, M. Greaves, G. M. Ganssen, H. Elderfield, and D. Kroon (2009), Western Arabian Sea SST during the penultimate interglacial: A comparison of U³⁷ and Mg/Ca paleothermometry, *Paleoceanography*, *24*, PA2212, doi:10.1029/2007PA001557.
- Schmiedl, G., and D. C. Leuschner (2005), Oxygenation changes in the deep western Arabian Sea during the last 190,000 years: Productivity versus deepwater circulation, *Paleoceanography*, *20*, PA2008, doi:10.1029/2004PA001044.
- Schmiedl, G., and A. Mackensen (2006), Multi-species stable isotopes of benthic foraminifers reveal past changes of organic matter decomposition and deepwater oxygenation in the Arabian Sea, *Paleoceanography*, *21*, PA4213, doi:10.1029/2006PA001284.
- Schmittner, A. (2005), Decline of the marine ecosystem caused by a reduction in the Atlantic overturning circulation, *Nature*, *434*, 628–633, doi:10.1038/nature03476.
- Schmittner, A., E. D. Galbraith, S. W. Hostetler, T. F. Pedersen, and R. Zhang (2007), Large fluctuations of dissolved oxygen in the Indian and Pacific oceans during Dansgaard-Oeschger oscillations caused by variations of North Atlantic Deep Water subduction, *Paleoceanography*, *22*, PA3207, doi:10.1029/2006PA001384.
- Schulz, H., R. von Rad, and H. Erlenkeuser (1998), Correlation between Arabian Sea and Greenland climate oscillations of the past 110,000 years, *Nature*, *393*, 54–57.
- Schulz, M., and M. Mudelsee (2002), REDFIT: Estimating red-noise spectra directly from unevenly spaced paleoclimatic time series, *Comput. Geosci.*, *28*(3), 421–426, doi:10.1016/S0098-3004(01)00044-9.
- Skinner, L. C., and N. J. Shackleton (2005), An Atlantic lead over Pacific deep-water change across Termination I: Implications for the application of the marine isotope stage stratigraphy, *Quat. Sci. Rev.*, *24*, 571–580, doi:10.1016/j.quascirev.2004.11.008.
- Spahni, R., et al. (2005), Atmospheric methane and nitrous oxide of the Late Pleistocene from Antarctic ice cores, *Science*, *310*(5752), 1317–1321, doi:10.1126/science.1120132.
- Spötl, C., A. Mangini, N. Frank, R. Eichstadter, and S. J. Burns (2002), Start of the last interglacial period at 135 ka: Evidence from a high Alpine speleothem, *Geology*, *30*(9), 815–818, doi:10.1130/0091-7613(2002)030<0815:SOTLIP>2.0.CO;2.
- Stott, L., C. Poulson, S. Lund, and R. Thunell (2002), Super ENSO and global climate oscillations at millennial time scales, *Science*, *297*(5579), 222–226, doi:10.1126/science.1071627.
- Thompson, W. G., and S. L. Goldstein (2006), A radiometric calibration of the SPECMAP time-scale, *Quat. Sci. Rev.*, *25*, 3207–3215, doi:10.1016/j.quascirev.2006.02.007.
- Tjallingii, R., M. Claussen, J.-B. Stuut, J. Fohlmeister, A. Jahn, T. Bickert, F. Lamy, and U. Rohl (2008), Coherent high- and low-latitude control of the northwest African hydrological balance, *Nat. Geosci.*, *1*, 670–675, doi:10.1038/ngeo289.
- Tuenter, E., S. L. Weber, F. J. Hilgen, L. J. Lourens, and A. Ganopolski (2005), Simulation of climate phase lags in response to precession and obliquity forcing and the role of vegetation, *Clim. Dyn.*, *24*, 279–295, doi:10.1007/s00382-004-0490-1.
- Turney, C. S. M., A. P. Kershaw, S. C. Clemens, N. Branch, P. T. Moss, and L. K. Fifield (2004), Millennial and orbital variations of El Niño/Southern Oscillation and high-latitude climate in the last glacial period, *Nature*, *428*, 306–310, doi:10.1038/nature02386.
- van Aken, H. M., H. Ridderinkhof, and W. P. M. de Ruijter (2004), North Atlantic deep water in the south-western Indian Ocean, *Deep Sea Res., Part I*, *51*(6), 755–776, doi:10.1016/j.dsr.2004.01.008.
- Wang, P., S. Clemens, L. Beaufort, P. Braconnot, G. Ganssen, Z. Jian, P. Kershaw, and M. Samthein (2005), Evolution and variability of the Asian monsoon system: State of the art and outstanding issues, *Quat. Sci. Rev.*, *24*, 595–629, doi:10.1016/j.quascirev.2004.10.002.
- Wang, Y. J., H. Cheng, R. L. Edwards, Z. S. An, J. Y. Wu, C.-C. Shen, and J. A. Dorale (2001), A high-resolution absolute-dated Late Pleistocene monsoon record from Hulu Cave, China, *Science*, *294*(5550), 2345–2348, doi:10.1126/science.1064618.
- Wang, Y., et al. (2005), The Holocene Asian monsoon: Links to solar changes and North Atlantic climate, *Science*, *308*(5723), 854–857, doi:10.1126/science.1106296.
- Wang, Y., H. Cheng, R. L. Edwards, X. Kong, S. Xiaohua, S. Chen, J. Wu, X. Jiang, X. Wang, and A. Zhisheng (2008), Millennial- and orbital-scale changes in the East Asian monsoon over the past 224,000 years, *Nature*, *451*, 1090–1093, doi:10.1038/nature06692.
- Webster, P. J., V. O. Magaña, T. N. Palmer, J. Shukla, R. A. Tomas, M. Yanai, and T. Yasunari (1998), Monsoons: Processes, predictability, and the prospects for prediction, *J. Geophys. Res.*, *103*(C7), 14,451–14,510, doi:10.1029/97JC02719.
- Winograd, I. J., T. B. Coplen, J. M. Landwehr, A. C. Riggs, K. R. Ludwig, B. J. Szabo, P. T. Kolesar, and K. M. Revesz (1992), Continuous 500,000-year climate record from vein calcite in Devils-Hole, Nevada, *Science*, *258*(5080), 255–260, doi:10.1126/science.258.5080.255.
- You, Y. (1998), Intermediate water circulation and ventilation of the Indian Ocean derived from water-mass contributions, *J. Mar. Res.*, *56*, 1029–1067, doi:10.1357/002224098765173455.
- Zahn, R., and T. F. Pedersen (1991), Late Pleistocene evolution of surface and mid-depth hydrography at the Oman Margin: Planktonic and benthic isotope records at Site 724, *Proc. Ocean Drill. Program Sci. Results*, *117*, 291–308.

- Ziegler, M., T. Jilbert, G. J. de Lange, L. J. Lourens, and G.-J. Reichart (2008), Bromine counts from XRF scanning as an estimate of the marine organic carbon content of sediment cores, *Geochem. Geophys. Geosyst.*, *9*, Q05009, doi:10.1029/2007GC001932.
- Ziegler, M., E. Tuenter, and L. J. Lourens (2010a), The precession phase of the boreal summer monsoon as viewed from the eastern Mediterranean (ODP Site 968), *Quat. Sci. Rev.*, *29*, 1481–1490, doi:10.1016/j.quascirev.2010.03.011.
- Ziegler, M., L. J. Lourens, E. Tuenter, and G.-J. Reichart (2010b), High Arabian Sea productivity conditions during MIS 13—Odd monsoon event or intensified overturning circulation at the end of the mid-Pleistocene transition?, *Clim. Past*, *6*, 63–76, doi:10.5194/cp-6-63-2010.
-
- F. Hilgen, L. J. Lourens, and G.-J. Reichart, Faculty of Geosciences, Utrecht University, Budapestlaan 4, NL-3584 CD Utrecht, Netherlands.
- E. Tuenter, Institute for Marine and Atmospheric Research Utrecht, Utrecht University, NL-3584 CC Utrecht, Netherlands.
- N. Weber, Chemistry and Climate Division, Royal Netherlands Meteorological Institute, PO Box 201, NL-3730 AE De Bilt, Netherlands.
- M. Ziegler, Lamont-Doherty Earth Observatory, Columbia University, Palisades, NY 10964, USA. (mziegler@ldeo.columbia.edu)